iScience

Article

LMO1 expression in neuroblastoma cells reprograms tumor-associated macrophages to promote metastasis

Graphical abstract

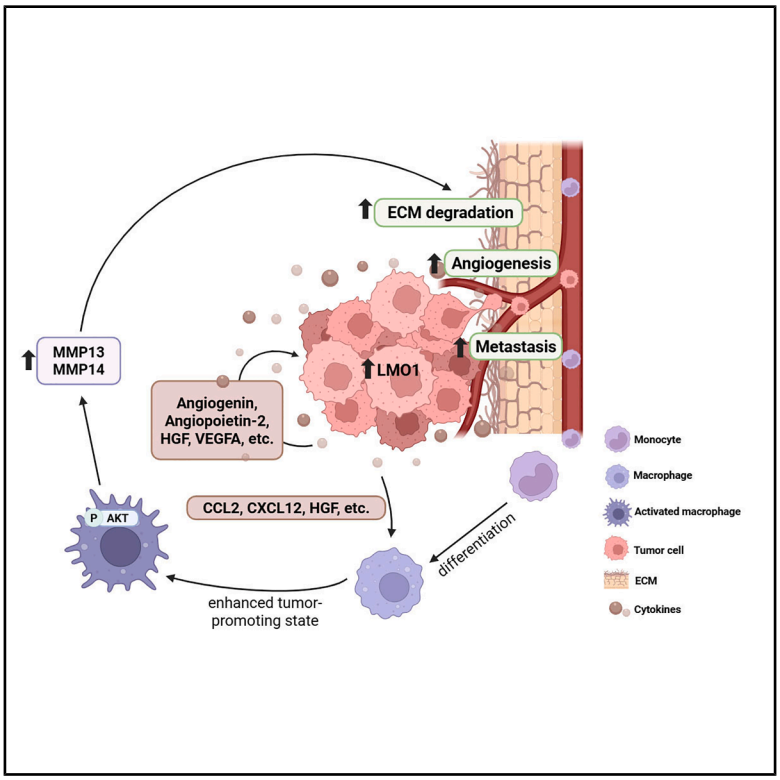

Highlights

- LMO1 accelerates metastasis of MYCN-driven neuroblastoma via macrophage remodeling
- LMO1 alters cytokines toward pro-metastatic signaling
- LMO1 boosts macrophage activity through PI3K-Akt-MMP pathways

Authors

Ke-En Tan, Zuag Paj Her, Cheng Zhang, ..., Thomas E. Rubino, Jr., Hu Li, Shizhen Zhu

Correspondence

zhu.shizhen@mayo.edu

In brief

Immunology; Cell biology; Cancer

Tan et al., 2026, iScience *29*, 115144
March 20, 2026
https://doi.org/10.1016/j.isci.2026.115144

CellPress

iScience

CellPress
OPEN ACCESS

Article

LMO1 expression in neuroblastoma cells reprograms tumor-associated macrophages to promote metastasis

Ke-En Tan,[1,2,5] Zuag Paj Her,[1,5] Cheng Zhang,[3] Kok Siong Yeo,[1] Taylor Weiskittel,[3] Cassie Howe,[1] Shyang Hong Tan,[3] Katherine M. Johnson,[1] Gina L. Razidlo,[1,4] Thomas E. Rubino, Jr.,[1] Hu Li,[3] and Shizhen Zhu[1,3,6,*]

[1]Department of Biochemistry and Molecular Biology, Mayo Clinic College of Medicine, Rochester, MN 55902, USA
[2]Institute of Biological Sciences, Faculty of Science, Universiti Malaya, Kuala Lumpur 50603, Malaysia
[3]Department of Molecular Pharmacology and Experimental Therapeutics, Center for Individualized Medicine, Mayo Clinic College of Medicine, Rochester, MN 55902, USA
[4]Division of Gastroenterology and Hepatology, Mayo Clinic, Rochester, MN 55902, USA
[5]These authors contributed equally
[6]Lead contact
*Correspondence: zhu.shizhen@mayo.edu
https://doi.org/10.1016/j.isci.2026.115144

SUMMARY

Neuroblastoma (NB) accounts for 10% of pediatric cancer-related deaths, is often highly metastatic at diagnosis, and has a 5-year-survival rate of <50% for patients with high-risk disease. We previously showed that the transcriptional coactivator LMO1 cooperates with the *MYCN* oncogene to enhance NB tumorigenesis and metastasis. To better understand this synergy, we performed single-cell RNA sequencing analysis on primary tumors from transgenic zebrafish overexpressing MYCN alone or with LMO1. Interestingly, we found that the macrophage populations from the two tumor types were transcriptionally distinct, and LMO1 increased cancer-cell secretion of cytokines associated with metastasis and angiogenesis. Conditioned media from LMO1-expressing NB cells activated PI3K-Akt signaling and MMP expression in human macrophages, enhancing matrix degradation and promoting NB cell migration *in vivo*. Our data suggest that LMO1 overexpression in *MYCN*-amplified NB cells increases the pro-metastatic properties of macrophages in the tumor-cell microenvironment, which is important for driving NB metastasis.

INTRODUCTION

As the most common extracranial solid tumor of the peripheral sympathetic nervous system in pediatric patients, neuroblastoma (NB) accounts for about 7% of all malignancies and 10% of cancer-related deaths in children.[1] The amplification of the *MYCN* oncogene is a hallmark of high-risk NB, occurring in about 25% of all NB cases.[2] Nearly half of children over 18 months of age with *MYCN* amplification present with widespread metastasis at diagnosis. Approximately 80% of patients with high-risk NB fail to respond to current intensive multimodal therapies, and survival for these patients is usually less than 50%.[3] This underscores the urgent need for developing safe and effective therapies for patients with NB and the importance of understanding the molecular basis of NB, particularly its tumor heterogeneity, highly metastatic nature, and the complex interactions between tumor cells and immune cells within the tumor microenvironment (TME).

Central to the current challenges with NB treatment is the heterogeneity of the NB molecular landscape that significantly contributes to NB pathogenesis. This includes somatic mutations, single-nucleotide polymorphisms (SNPs), DNA ploidy, chromosomal alterations, and aberrant regulation of gene expression. Our studies and reports from others, using zebrafish and mouse models, have demonstrated that multiple genetic aberrations, including activated *ALK* and *PTPN11*, overexpression of *LMO1*, *MYC*, *GAB2*, *PA2G4*, *DEF*, and *DLST*, and loss of function of *gas7*, *nf1*, *arid1a*, *Caspase 8*, promote NB tumorigenesis and/or metastasis either alone or in cooperation with *MYCN*.[4–7] Among all NB-relevant genes, the LIM-domain only 1 gene (*LMO1*), which encodes a transcriptional coregulator, was one of the key genes identified from a successful NB genome-wide association study.[8] SNPs in the super-enhancer region of *LMO1* (e.g., rs110419 and rs2168101) and duplication of the *LMO1* locus (11p15.4) have been associated with more advanced NB and worse outcome.[8,9] Beyond NB, LMO1's oncogenic role extends to hematological malignancies, including T cell acute lymphoblastic leukemia and T cell lymphoma. Through oncogenic reprogramming of thymocytes, aberrant expression of LMO1 activates the self-renewal machinery and malignant transformation.[10,11] Moreover, LMO1 was recently reported to promote the development of gastric cancer, lung cancer, colorectal cancer, prostate cancer, and glioblastoma by regulating the expression of tumor-progression-related genes,

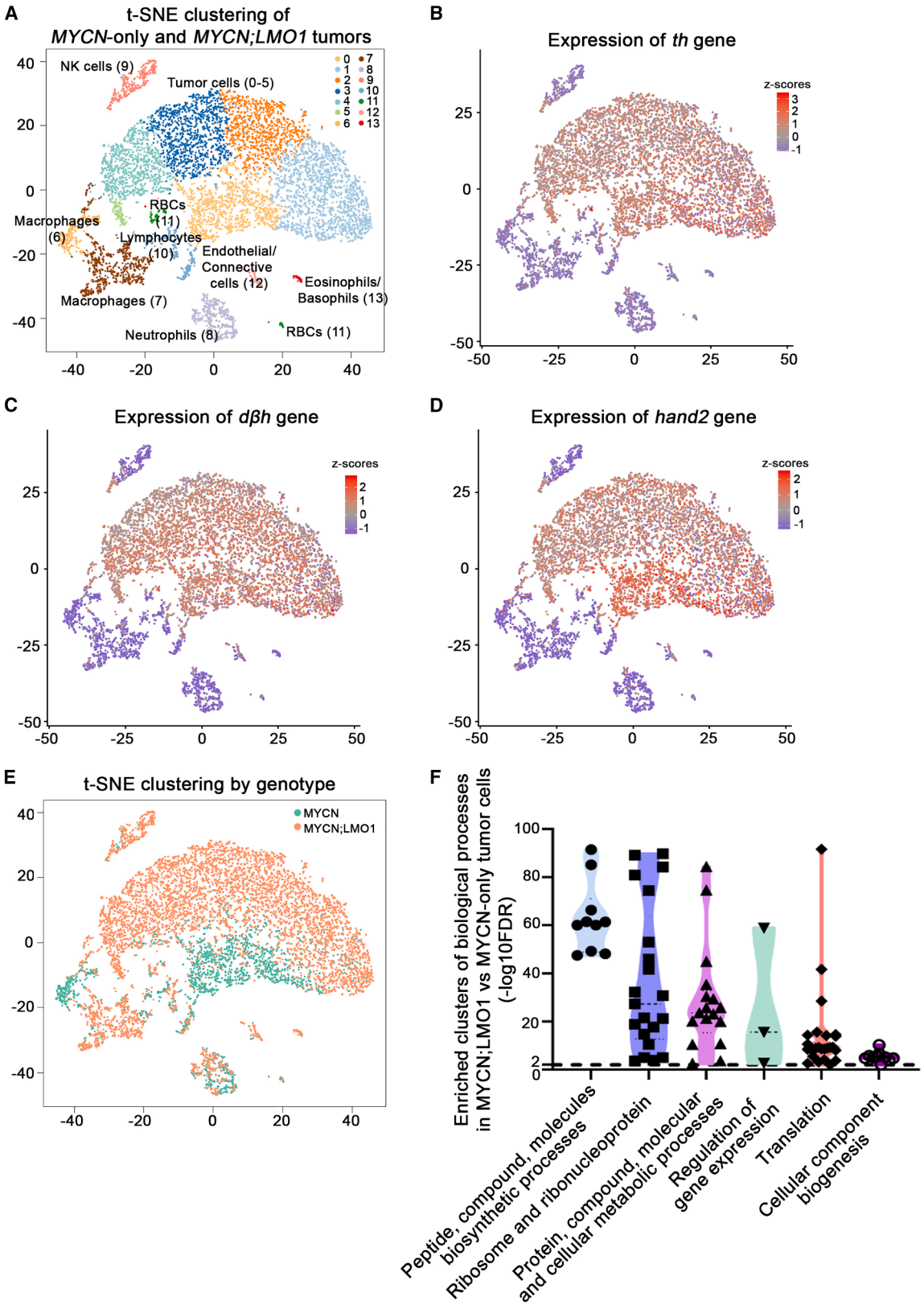

(legend on next page)

such as *p21*, *PSA*, *Bcl-2*, *Bax,* and *TTK/MPS1*.[12,13] Thus, LMO1 appears to be a potent driver of cancer progression in general.

In a prior study using a zebrafish model of NB that we developed,[14] we showed that the overexpression of LMO1 synergizes with MYCN to significantly enhance tumor progression and metastasis *in vivo*. Although LMO1 is not a transcriptional target of MYCN, coexpression of LMO1 with MYCN i) accelerated tumor development and increased disease penetrance, ii) promoted cell invasion/migration *in vitro* and metastasis *in vivo*, and iii) upregulated genes involved in cell-matrix interactions to enhance the stiffness of extracellular matrix (ECM). To further understand whether LMO1-overexpressing tumor cells impact the TME to facilitate metastasis, especially through interactions with non-tumor cells, we performed single-cell RNA sequencing (scRNA-seq) analysis on primary tumors derived from transgenic zebrafish driven by the overexpression of MYCN, either alone (referred to hereafter as the "*MYCN*" line) or in combination with LMO1 (referred to hereafter as the "*MYCN; LMO1*" line). Interestingly, we found distinct populations of macrophages from each tumor type using a t-distributed stochastic neighbor embedded (t-SNE) clustering approach. We found that LMO1 overexpression modifies the cancer-cell secretome to elevate levels of cytokines that promote tumor growth, metastasis, and angiogenesis. Macrophages cultured with conditioned media derived from LMO1-overexpressing human *MYCN*-amplified NB cells upregulated matrix metalloproteinases (MMPs), possibly through PI3K-Akt activation, and were better able to degrade matrix and promote the *in vivo* migration/invasion of NB cells. Our data therefore suggest that LMO1 overexpression in *MYCN*-amplified NB cells changes the functionality of tumor-associated macrophages to promote NB progression and metastasis.

RESULTS

Single-cell RNA sequencing-seq analysis shows significantly enriched signaling pathways involved in biogenesis and metabolism in neuroblastoma cells with the overexpression of LIM-domain only 1 gene and MYCN

To better understand whether NB cells with the overexpression of LMO1 could modify the TME to favor tumor progression and metastasis, we performed individual scRNA-seq on primary tumors isolated from three *MYCN;LMO1* compound transgenic fish and two *MYCN*-only transgenic fish, all aged 6–8 months. Notably, all three *MYCN;LMO1* fish exhibited distant metastasis originating from the primary tumor site in the head kidney region, whereas no observable tumor metastases were detected in the MYCN-only fish. A total of 16630 cells were sequenced, yielding 9082 high-quality transcriptomes after quality control and filtering (Figures S1A and S1B; Tables S1 and S2). Subsequent hierarchical clustering and pseudobulk analyses followed by DESeq2 comparison indicated that the differences observed between *MYCN* and *MYCN;LMO1* tumor samples were driven by underlying biological variation rather than technical batch effects (Figures S1C and S1D). Using t-SNE clustering with 10 principal components on pooled data from the five tumors, we identified 13 cell subpopulations in these tumor masses with 6 clusters as tumor-cell populations and 7 clusters as non-tumor-cell populations (Figure 1A; Figure S1A; Table S2). As the major components of the tumor masses, clusters 0–5 uniquely express high levels of NB-specific marker genes,[15] including *th*, *dβh,* and *hand2* genes (Figures 1B–1D), thus confirming their NB-cell identity. In addition, we found that tumor cells expressing MYCN alone (mainly in cluster 0) are distinctly clustered from those expressing both MYCN and LMO1 (mainly in clusters 1–5 (Figure 1E**)**). Gene ontology (GO) pathway enrichment analysis of genes significantly overexpressed in *MYCN;LMO1* tumor cells, using either the full dataset or a downsampled dataset with cell numbers matched to the *MYCN*-only group, consistently showed that *MYCN;LMO1* tumors are highly enriched for pathways involved in biosynthesis and metabolism, such as i-ii) peptide, compound, molecules biosynthetic and metabolic processes, iii) ribosome and ribonucleoprotein complex assembly and biogenesis, iv) regulation of gene expression, v) translation, and vi) cellular component biogenesis (Figure 1F**;** Tables S3 and S4). The top 12 significantly differentially expressed genes contributing to multiple GO categories are presented in Figure S3. Notably, these enriched metabolic, cellular, and biological processes in *MYCN;LMO1* tumors have been reported to be correlated with increased tumor aggressiveness and poor clinical outcomes across multiple cancer types.[16–21] These observations align with the heightened aggressiveness of *MYCN;LMO1* tumors compared with *MYCN*-only tumors that we previously observed in our transgenic zebrafish models.[14]

Macrophages derived from *MYCN;LMO1* tumors show features that are distinct from *MYCN*-only tumors

In addition to tumor-cell populations, we also identified 7 non-tumor-cell populations, including macrophages (clusters 6 and 7), neutrophils (cluster 8), natural-killer (NK) cells (cluster 9), lymphocytes (cluster 10), red blood cells ("RBCs", cluster 11),

Figure 1. Tumor cells expressing MYCN alone or MYCN plus LMO1 are clustered into distinct subpopulations via single-cell RNA sequencing analysis

(A) Primary NB tumors from *MYCN* ($n = 2$) and *MYCN;LMO1* ($n = 3$) zebrafish lines were analyzed by single-cell RNA-sequencing (scRNA-seq) using a t-distributed stochastic neighbor embedding (t-SNE clustering) method. Pooled scRNA-seq data from the 5 tumors is displayed as 13 distinct phenotypic clusters: tumor cells (clusters 0, 1, 2, 3, 4, and 5); macrophages (clusters 6 and 7); neutrophils (cluster 8); natural-killer (NK) cells (cluster 9); lymphocytes (cluster 10); erythrocytes ("RBCs," cluster 11); endothelial and/or connective tissue cells (cluster 12); and eosinophils/basophils (cluster 13).

(B–D) t-SNE clustering plot of pooled scRNA-seq data from panel A showing NB marker gene expression for *th* (B), *dβh* (C), and *hand2* (D). *dβh*, dopamine beta hydroxylase; *hand2*, heart and neural crest derivatives expressed 2; *th*, tyrosine hydroxylase.

(E) t-SNE clustering plot of pooled scRNA-seq data from panel A, coloring cells according to host genotype.

(F) Significantly enriched pathways sharing similar Gene Ontology (GO) terms in *MYCN;LMO1* vs. *MYCN*-only tumor cells were consolidated into broader functional categories. For each category, the -log10(FDR) values of the constituent pathways were visualized as violin plots, with only pathways exceeding a threshold of $\log_{10}(FDR) > 2$ included.

endothelial/connective cells (cluster 12), and eosinophils/basophils (cluster 13), using overrepresentation analysis (Figures 1A; Figure S2B and S2C) and the SciBet algorithm (Figure S2D) with signature gene sets of known tissue- and cell-type-specific markers.[22] Interestingly, we found that macrophages derived from the *MYCN*-only tumors account for 91% of total cells in cluster 6 and are distinctly clustered from those derived from *MYCN;LMO1* tumor masses, which accounted for 86% of total cells in cluster 7 (Figures 2A and 2B). In addition, our GO pathway enrichment analyses with significantly upregulated genes in cluster 7 versus cluster 6 showed dramatically enriched pathways involved in metabolism and biogenesis, such as i) ribonucleoprotein complex and biogenesis, ii) organic compound metabolic process, iii) protein, ATP and nucleotide metabolic processes, iv) translation, v) respiration, vi) oxidative phosphorylation, and vii) proton and electron transport (Figure 2C; Tables S5 and S6).

In a microenvironment, macrophages could generally exist in two polarized states depending on the presence of diverse cytokines and antigens, i.e., classically activated macrophages (M1) and alternatively activated macrophages (M2). M1 macrophages typically exhibit anti-inflammatory properties and play key roles in anti-tumor as well as anti-bacterial activities. In contrast, M2 macrophages are primarily involved in tissue remodeling, immunomodulation, and are often presented with pro-tumor characteristics by supporting tissue repair and promoting tumor progression. Tumor-associated macrophages (TAMs) frequently resembles M2-like phenotypes, contributing to an immunosuppressive TME that favors tumor growth and enables immune evasion.[23] To examine whether macrophages derived from *MYCN;LMO1* tumor fish lose an M1-like phenotype or acquire M2-like characteristics, we calculated gene set variation analysis (GSVA) score for each group using selected M1 and M2 signature genes conserved across zebrafish, mouse, and human (Figures 2D and 2F). The analysis revealed that cluster-7 macrophages exhibited a significantly lower M1 GSVA score compared with cluster-6 macrophages, where no significant difference was observed in M2 GSVA scores. The expression patterns of individual M1 and M2 marker genes between the two clusters are presented in Figures 2E and 2G. Since only a limited number of M1/M2-fate-determining signature genes are both zebrafish-conserved and suitable for computational analysis, these data alone may not be sufficient to conclude that LMO1 induces major shifts in macrophage polarization in MYCN-driven tumors. However, our pathway-enrichment analysis using the full dataset or a downsampled dataset revealed a significant increase in metabolism and biogenesis pathways in cluster-7 macrophages, suggesting that LMO1 overexpression in MYCN-expressing NB cells may influence macrophage activity or function in a way that promotes tumor progression.

Macrophages cultured with conditioned media derived from LIM-domain only 1 gene-overexpressing NB cells accelerate tumor-cell migration *in vivo*

To examine whether LMO1-overexpressing NB cells alter macrophage activity to facilitate tumor metastasis, we collected conditioned media (CM) from a control human *MYCN*-amplified NB cell line called BE2C (“Ctl CM”), which expresses relatively low levels of endogenous LMO1, and from LMO1-overexpressing BE2C cells (“LMO1 CM”) to culture U937 human monocytes after PMA-induced differentiation to M0 macrophages (Figure 3A). CM-treated macrophages were then labeled with ViaFlour-405-blue-fluorescent dye and co-injected with mCherry-labeled control BE2C cells into the perivitelline space (PVS) of 2-day-old AB wild-type zebrafish embryos that had been treated with PTU to inhibit pigment formation. Migration of the co-injected tumor cells and CM-treated macrophages in zebrafish larvae was monitored by fluorescence microscopy at 1 and 3-4 days post injection (dpi) (Figures 3B–3I). Among the 55 larvae injected with Ctl-CM-treated macrophages plus BE2C cells, 12 larvae (22%) showed the migration of mCherry-labeled BE2C cells away from the injection site at 3-4 dpi (Figures 3B , 3C, 3F, 3G, and 3J). Strikingly, 50 out of 55 larvae (91%) injected with LMO1-CM-treated macrophages plus BE2C cells showed spreading of mCherry-labeled BE2C cells far from the injection site (Figures 3D, 3E, 3H, 3I, and 3J). These data suggest that LMO1 expression in *MYCN*-amplified NB cells causes them to secrete factors into the tumor-cell microenvironment that enhance the migration-promoting ability of macrophages.

Macrophages cultured with conditioned media from LIM-domain only 1 gene-overexpressing neuroblastoma cells upregulate matrix metalloproteinases expression and increase their matrix-degrading ability

TME, which includes ECM and stromal cells, is important for tumor development and progression.[24] TAMs can remodel the ECM by manipulating the expression and activity of MMPs to accelerate tumor metastasis.[25] In our scRNA-seq analyses, we observed increased expression levels of *mmp9*, *mmp13a,* and *mmp14b* (the zebrafish orthologs of human *MMP9*, *MMP13,* and *MMP14*, respectively) in the cluster-7 (*MYCN;LMO1*-predominant) macrophages compared to cluster-6 (*MYCN*-only-predominant) macrophages (Figures 4A and 4B). Consistently, qRT-PCR and western blot analysis showed significant upregulation of *MMP13* and *MMP14* in LMO1-CM-treated macrophages compared to Ctl-CM-treated macrophages (Figures 4C and 4E). To examine whether the upregulation of MMPs in LMO1-CM-treated macrophages promotes their ECM degradation activity, we performed a gelatin degradation assay with ViaFlour-405-fluorescent-dye-labeled macrophages treated with either Ctl CM or LMO1 CM. LMO1-CM-treated macrophages exhibited stronger gelatin degradation (∼2-fold), with an average degradation area of 0.47% per cell, compared to 0.28% per cell by Ctl-CM-treated macrophages (Figure 4D).

Since PI3K-Akt pathway activation in macrophages is an essential step in facilitating tumor metastasis, and this pathway is known to regulate the expression of multiple MMPs,[26,27] we examined whether the PI3K-Akt pathway is activated in LMO1-CM-treated macrophages. Western blotting analysis on lysates from Ctl-CM-treated or LMO1-CM-treated U937 macrophages showed increased levels of phosphorylated Akt in the LMO1-CM-treated macrophages, suggesting that PI3K-Akt pathway activation in macrophages may enhance their ability to degrade ECM and promote cancer-cell invasion by increasing MMP expression. To further validate the role of the PI3K-Akt-MMP axis in regulating macrophage activity during tumor metastasis,

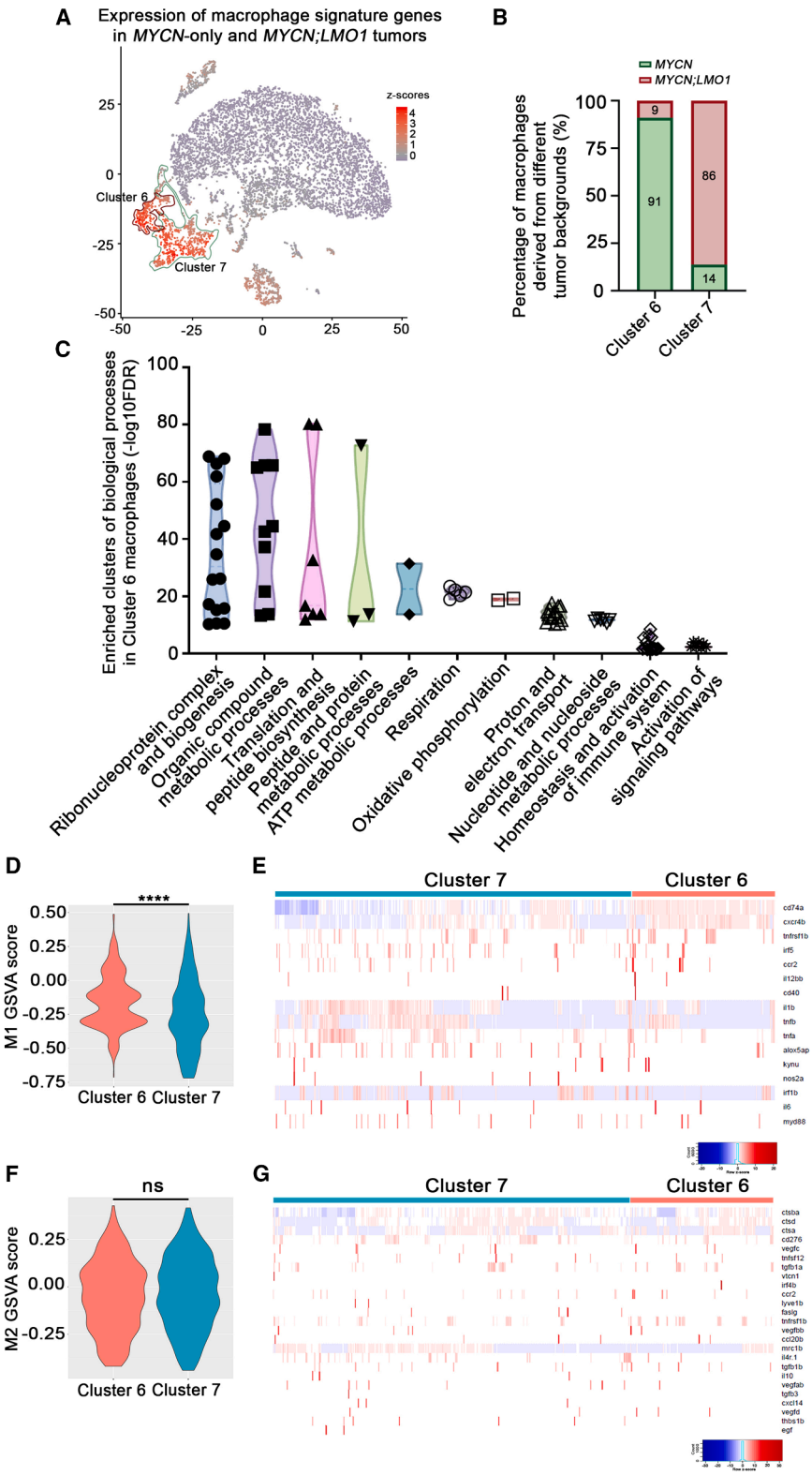

Figure 2. Macrophages derived from *MYCN;LMO1* tumors are distinct from *MYCN*-tumor-associated macrophages

(A) t-SNE clustering plot of pooled scRNA-seq tumor data from Figure 1A shows macrophage signature gene expression in *MYCN* tumors ($n = 2$) and *MYCN;LMO1* tumors ($n = 3$).

(B) Quantitation of macrophages derived from *MYCN* or *MYCN;LMO1* tumors in clusters 6 and 7 from panel A.

(C) Violin plots of significantly enriched biological processes in cluster-6 vs. cluster-7 macrophages from panel A with $\log_{10}$ FDR >2.

(D) GSVA scores reflect M1 polarization status in cluster-6 and cluster-7 macrophages, $^{****}p < 0.0001$.

(E) Heatmap displays the expression of M1 signature genes in cluster-6 and cluster-7 macrophages.

(F) GSVA scores reflect M2 polarization status in cluster-6 and cluster-7 macrophages. ns, not significant.

(G) Heatmap displays the expression of M2 signature genes in cluster-6 and cluster-7 macrophages.

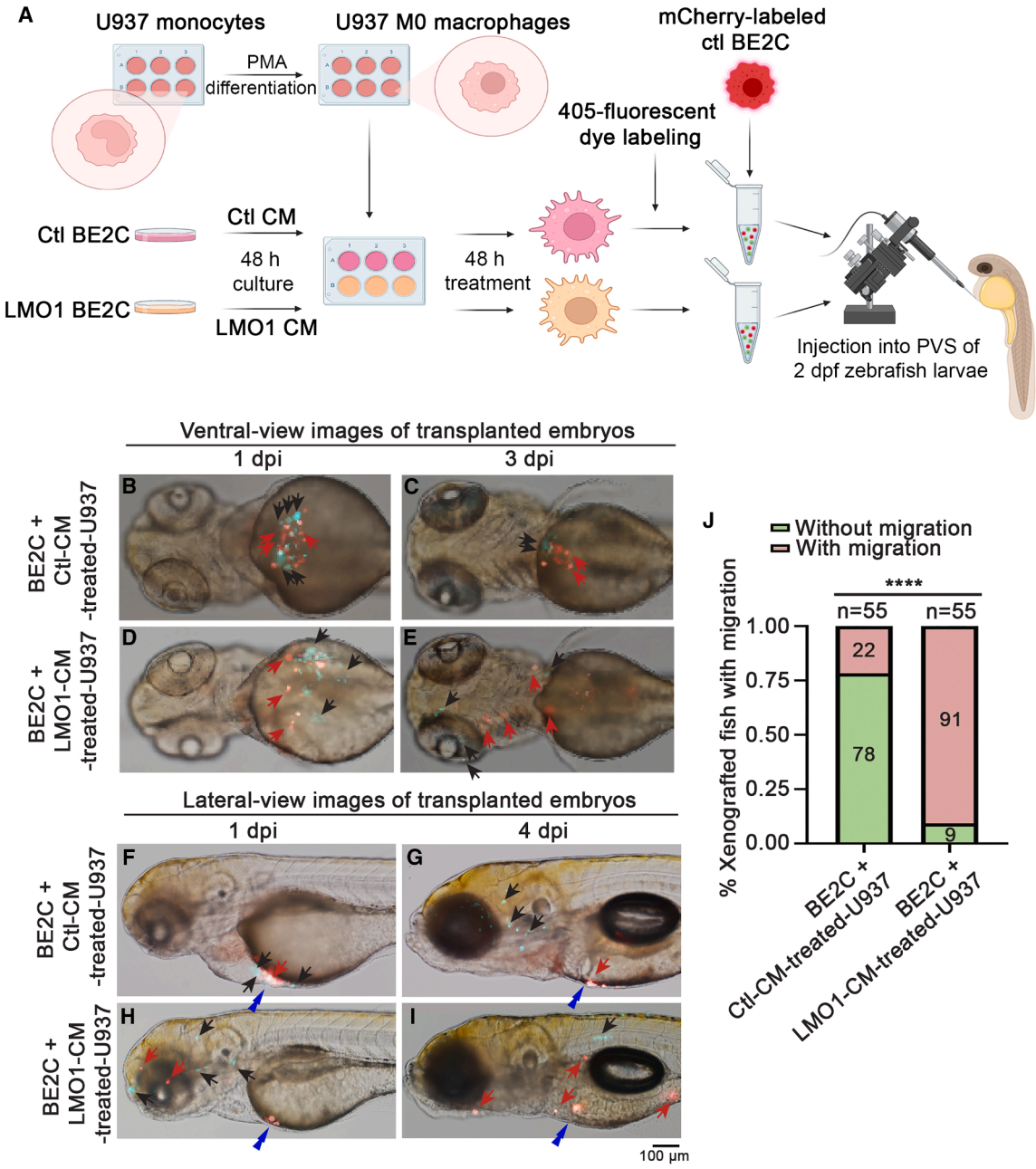

Figure 3. Macrophages cultured with conditioned media from LMO1-overexpressing BE2C cells accelerate tumor-cell migration *in vivo*

(A) Schematic diagram of experimental setup. U937 human monocytes were first differentiated to M0 macrophages with phorbol 12-myristate 13-acetate (PMA) and then cultured in conditioned media (CM) derived from control ("Ctl") or LMO1-overexpressing ("LMO1") BE2C cells. Ctl-CM-treated and LMO1-CM-treated U937 cells were labeled with ViaFluor 405 (green-fluorescent) dye. Each group of 405-labeled U937 cells was then combined with mCherry-labeled BE2C cells and co-injected into 2-day-old zebrafish through the perivitelline space (PVS, see diagram for the location of injection).

(B–I) Ventral-view (B-E) or lateral-view (F-I) fluorescent images of transplanted zebrafish larvae at 1 day post-injection (dpi, left panels) or 3–4 dpi (right panels) (scale bars, 100 μm). Blue double arrowheads point to the site of injection in panels B-E. Black arrows point to U937 macrophages. Red arrows point to BE2C NB cancer cells.

(J) Quantification of transplanted fish with NB cell migration ($n = 55$). Migration of NB cells in transplanted recipients was defined as at least one or more mCherry-positive tumor cells located in the anterior regions of the fish, distant from the site of injection (outside of PVS and yolk). ****$p \leq 0.0001$.

macrophages cultured with LMO1-CM were treated with the Akt inhibitor Miransertib.[28] Macrophages exposed to LMO1-CM and Miransertib exhibited a significant reduction in MMP13 and MMP14 expression at both RNA and protein levels (Figure 5A and 5B). Consistently, Miransertib-treated macrophages displayed a reduced area of gelatin degradation, demonstrating

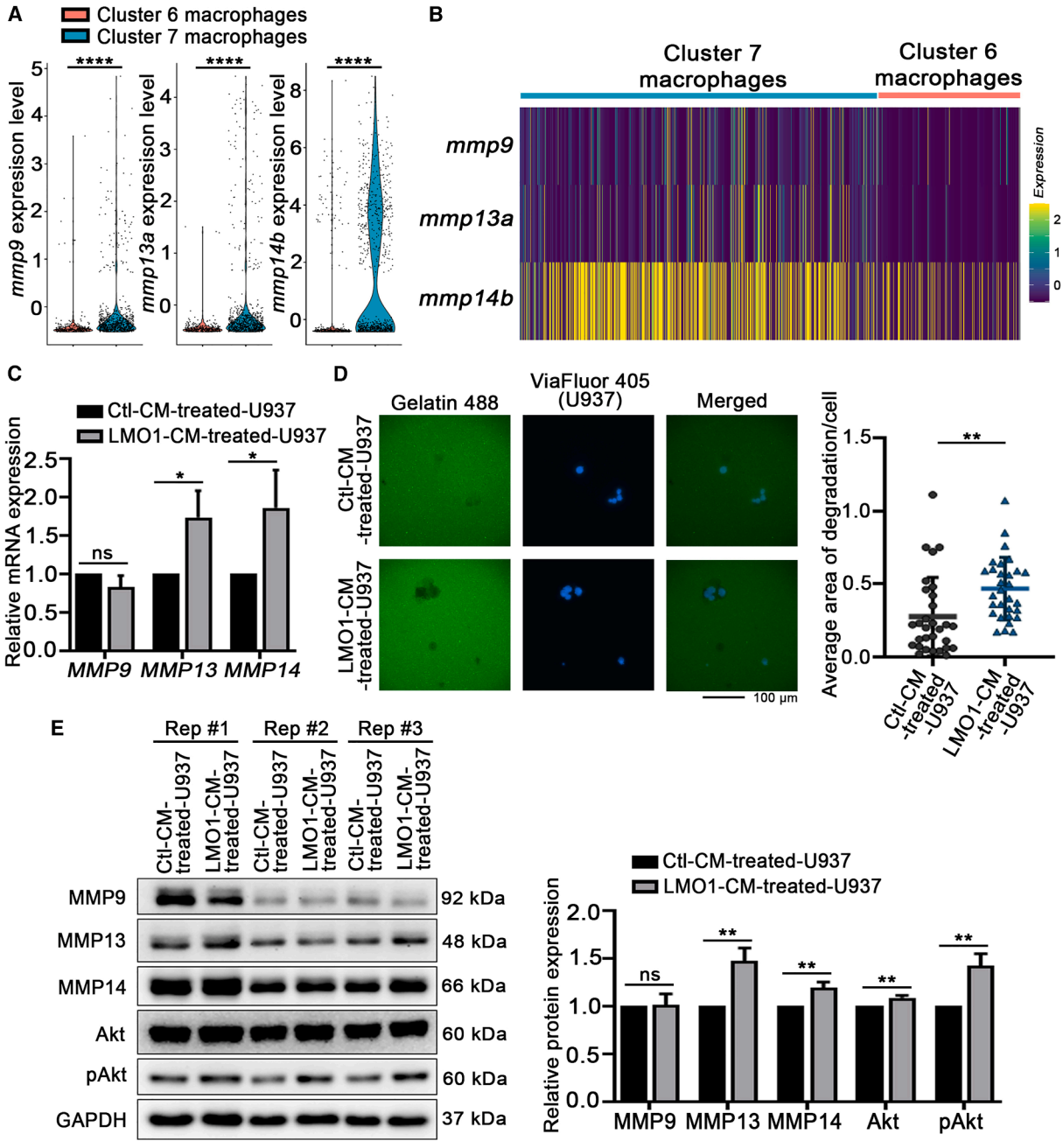

Figure 4. Macrophages cultured with CM derived from LMO1-overexpressing NB cells show increased gelatin degradation and activation of the PI3K-AKT pathway

(A) Normalized expression of *mmp9*, *mmp13a,* and *mmp14b* in macrophages from Clusters 6 and 7 in the sc-RNAseq dataset. Gene expression values were normalized using Seurat's LogNormalize method (scaled to 10,000 total counts per cell and log-transformed).

(B) Heatmap displays the expression of *mmp9*, *mmp13a,* and *mmp14b* in cluster-6 and cluster-7 macrophages from the scRNAseq data.

(C) RT-qPCR analysis of *MMP* gene expression levels in Ctl-CM-treated and LMO1-CM-treated U937 cells ($n = 4$).

(D) ViaFlour-405-labeled U937 cells that were cultured with Ctl CM or LMO1 CM (see Figure 3A) were analyzed for their ability to degrade matrices using a gelatin degradation assay ($n = 3$, scale bars, 100 µm). Gelatin was labeled with GFP. Its degradation causes loss of GFP expression and leaves black marks. Right panel shows the quantification of the degraded area of gelatin.

(E) Western blotting analysis of protein lysates from Ctl-CM-treated and LMO1-CM-treated U937 cells using antibodies against pAkt and Akt ($n = 3$). Expression of GAPDH was included as a loading control. Rep #1, Rep #2, and Rep #3 refer to three independent experiments. The right panel shows the quantification of protein expression from data in (E). Data in (C, D, and E) are presented as mean ± SD. *$p \leq 0.05$, **$p \leq 0.01$, and ****$p \leq 0.0001$.

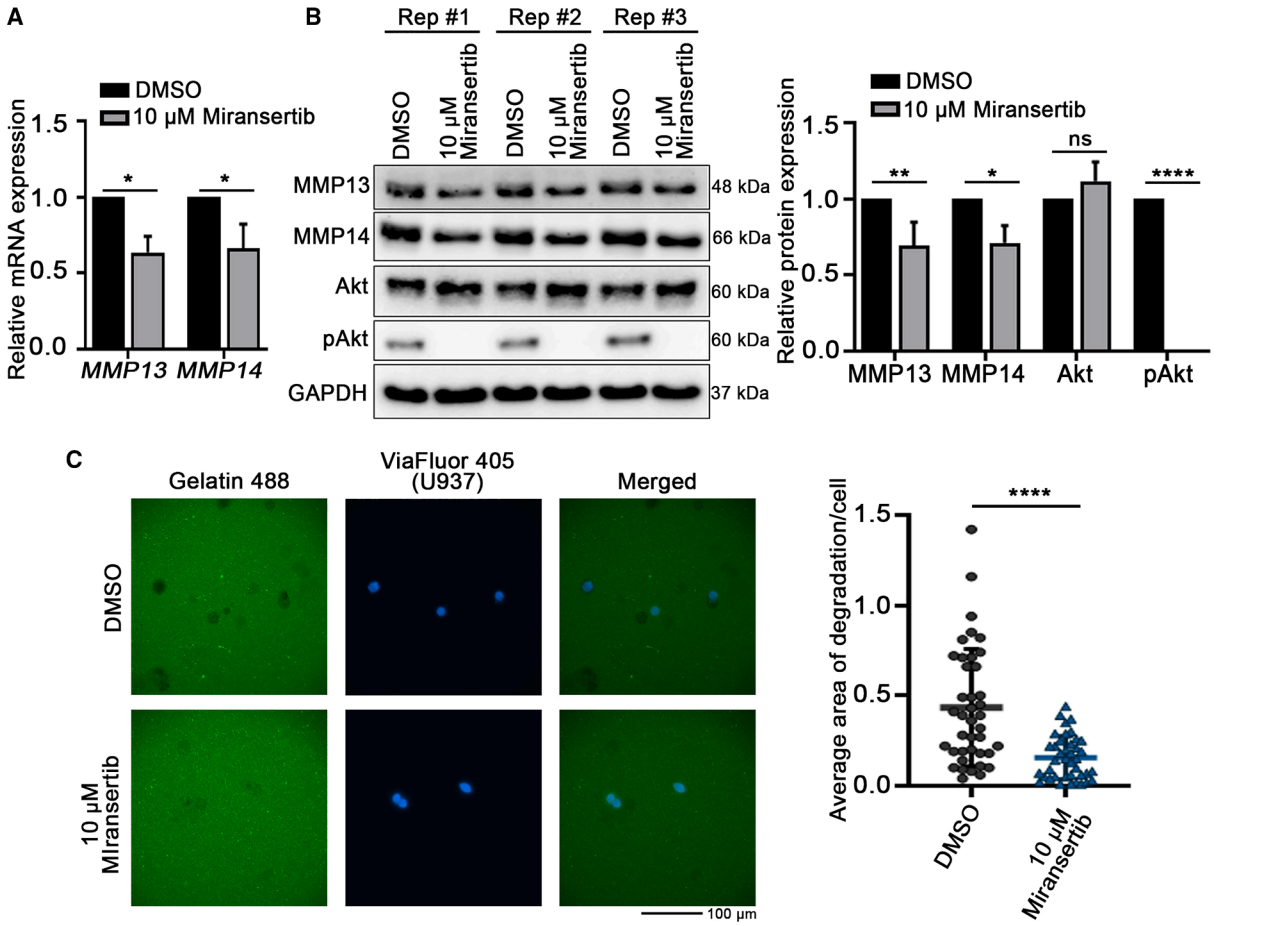

Figure 5. Akt inhibitor treatment reduces MMP expression and gelatin-degrading activity in macrophages cultured with LMO1-CM

(A) RT-qPCR analysis of *MMP* gene expression levels in U937 cells treated with LMO1-CM, with and without Akt inhibitor (10 μM Miransertib) (n = 3–4).

(B) Western blotting analysis of protein lysates from LMO1-CM-treated U937 cells, with or without Akt inhibitor, using antibodies against MMP13, MMP14, pAkt, and Akt ($n = 3$). Expression of GAPDH served as a loading control. Rep #1, Rep #2, and Rep #3 refer to three independent experiments. Right panel shows the quantification of protein expression.

(C) Assessment of gelatin degradation by U937 cells (labeled with ViaFluor-405) cultured with LMO1-CM in the presence or absence of an Akt inhibitor ($n = 4$, scale bars, 100 μm). The right panel shows the quantification of the degraded gelatin area. Data in panels C are presented as mean ± SD. $^{*}p \leq 0.05$, $^{**}p \leq 0.01$, and $^{***}p \leq 0.0001$.

that Akt activation in macrophages contribute ECM modulation through MMPs (Figure 5C).

Pro-tumor-cytokine levels are increased in the conditioned media from LIM-domain only 1 gene-overexpressing neuroblastoma tumor cells

To promote tumor growth and metastasis, tumor cells release cytokines to attract and impact a variety of immune and stromal cells.[29] To identify potential metastasis-promoting cytokines secreted from LMO1-overexpressing NB cells, CM from control or LMO1-overexpressing BE2C cells was collected 48 h after cell seeding and used to probe cytokine arrays that have the capacity to simultaneously detect 105 cytokines. After normalizing these arrays using the internal controls loaded at the corners of the blots, we detected elevated levels of the following cytokines in LMO1 CM: Angiogenin, Angiopoietin-2, CD14, EGF, Endoglin/CD105, GDF-15, HGF, ICAM-1/CD54, CCL2/MCP-1, CXCL12/SDF-1 alpha and VEGFA (Figures 6A and 6B; Figure S4). To validate that the increased cytokine levels correlate with their transcriptional upregulation in LMO1-overexpressing cells, we performed qRT-PCR analysis on both control and LMO1-overexpressing BE2C cells. Consistently, we detected the significant upregulation of most of these cytokine-encoding genes in BE2C cells with LMO1 overexpression (Figure 6C). Many of these enriched cytokines, including CCL2, CXCL12, ANGPT2, VEGFA, and HGF, are known to promote tumor growth, angiogenesis, chemotaxis of immune cells, and polarization of macrophages.[30–32] These data are consistent with a model whereby LMO1 overexpression in NB cells causes the release of tumor-promoting cytokines from NB cells that lead to PI3K pathway activation and MMP expression in macrophages, thereby promoting ECM remodeling, tumor-cell invasion and dissemination, and metastatic progression (Figure 7).

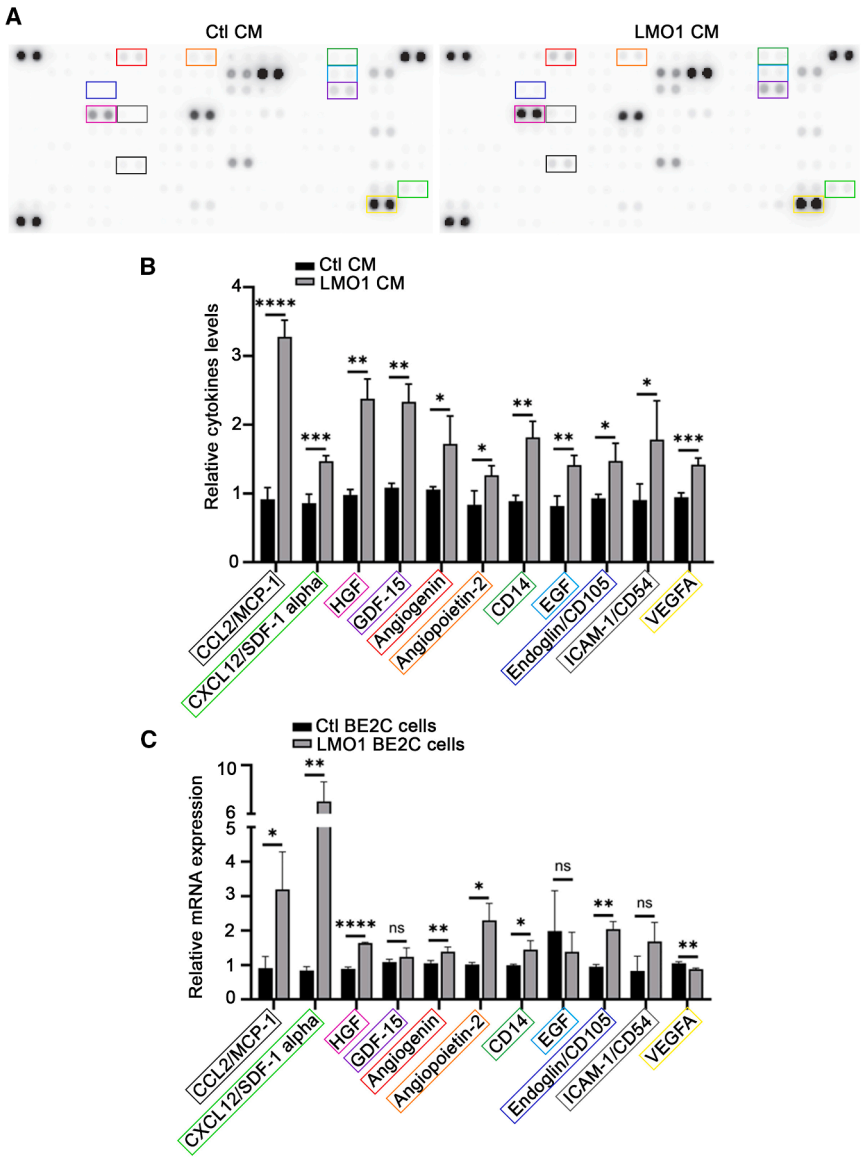

Figure 6. Increased levels of metastasis-promoting cytokines are detected in the CM derived from LMO1-overexpressing BE2C cells

(A) Cytokine arrays were probed using CM from Ctl BE2C cells (left) and LMO1-overexpressing BE2C cells (right) (n = 2). Metastasis-promoting cytokines are labeled as follows: red boxes - Angiogenin; orange boxes - angiopoietin-2; green boxes - CD14; light-blue boxes - EGF; dark-blue boxes - Endoglin/CD105; purple boxes - GDF-15; pink boxes - HGF; gray boxes - ICAM-1/CD54; black boxes - CCL2/MCP-1; neon-green boxes - CXCL12/SDF-1 alpha; yellow boxes - VEGFA.

(B) Quantitation of relative cytokine levels based on the normalized signal intensity on two independent cytokine array blots (n = 2).

(C) Relative expression of genes (determined by qRT-PCR) encoding the indicated cytokines in Ctl and LMO1-overexpressing BE2C cells (n = 4). Data in (B) and (C) are presented as mean ± SD. *$p \leq 0.05$, **$p \leq 0.01$, ***$p \leq 0.001$, and ****$p \leq 0.0001$. ns; not significant.

DISCUSSION

MYCN amplification is one of the earliest genetic markers discovered in NB. It continues to be useful for the stratification of NB stages and is one of the strongest predictors of poor prognosis in patients with NB.[33] Yet, murine and zebrafish animal NB models driven by MYCN overexpression alone seldomly metastasize.[34] Our previous work showed that LMO1 synergizes with MYCN to accelerate the tumor onset, penetrance and metastasis of NB cells by promoting their migration and invasion abilities, as well as increasing the stiffness of the ECM.[14] Disassembly of the ECM by MMPs and other enzymes is required for tumor invasion and dissemination,[35] and elevated MMP levels have been associated with poor prognosis in various cancers.[36] Consistently, our findings show that MMP9, MMP13 and MMP14 are upregulated in macrophages by exposure to CM from LMO1-expressing NB cells, likely driving the enhanced ability of these macrophages to degrade matrix and further demonstrating the cooperative interaction between tumor cells and macrophages in TME modification. The activated PI3K-Akt signaling in the LMO1-CM-treated macrophages is consistent with previous work showing that the activation of this pathway in phagocytes upregulates the transcription of essential genes for tumor metastasis, such as VEGFA[37,38] and MMP9.[27,39] Activation of the PI3K-Akt pathway has also been shown to promote the alternative activation of macrophages through reduced M1 polarization[40] and could contribute to the phagocytotic ability and survival of macrophages, as well as disease progression.[41,42] Thus, the PI3K-Akt pathway could be important for pro-metastatic communication between NB cells and TAMs.

The remodeling of the ECM alone is likely to be insufficient to trigger the departure of tumor cells from the primary tumor site. Cytokines that usually act in both paracrine and autocrine manners with a feedback mechanism are also likely to be important for tumor-cell invasion and dissemination. Along with the rapid proliferation of tumor cells, prolonged cytokine exposure causes loss of immune homeostasis, eventually leading to a chronically inflamed, tumor-friendly environment. Our cytokine arrays revealed that LMO1 overexpression caused a shift in the cancer-cell secretion of angiogenesis-related cytokines. Angiogenesis is orchestrated by both pro-angiogenic and anti-angiogenic factors, and an imbalance in these factors can promote pathological states of angiogenesis. Angiogenin was the first-discovered human angiogenic factor shown to promote tumor proliferation and

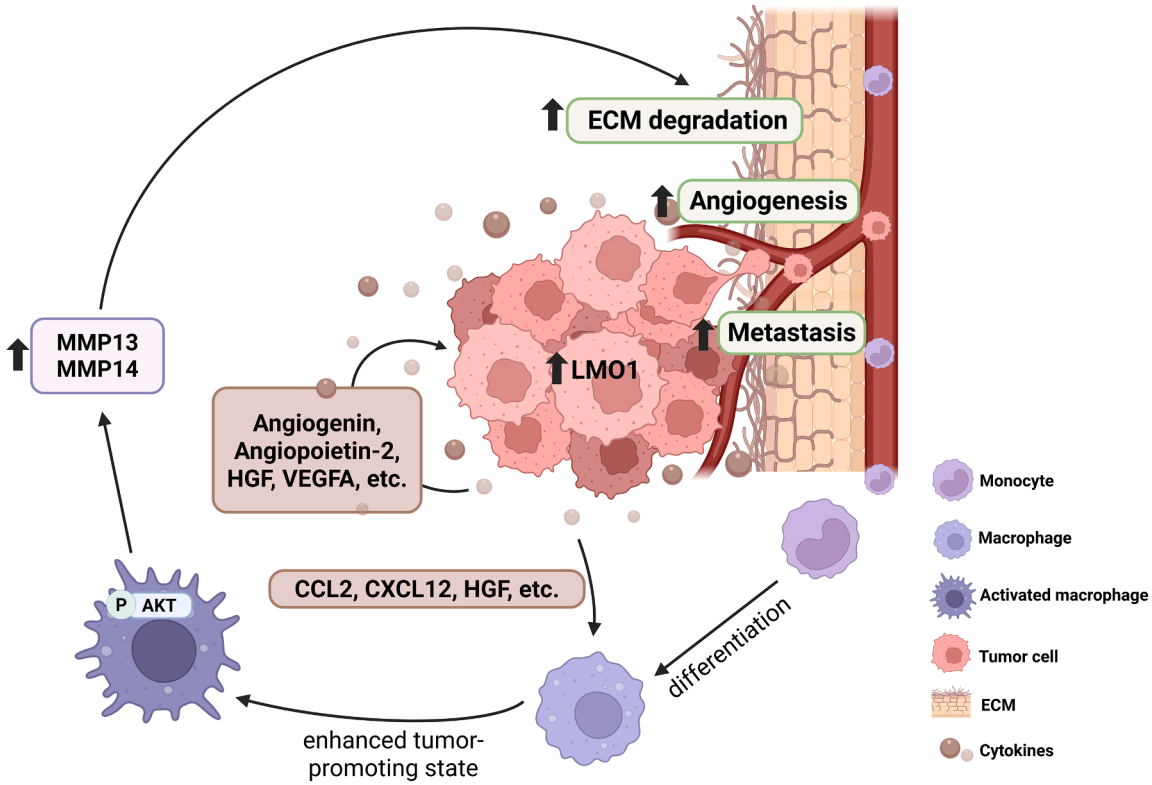

Figure 7. A proposed model illustrates the interplay between LMO1-overexpressing human NB cells and the tumor microenvironment during metastasis

Overexpression of LMO1 in NB cells increases the secretion of cytokines that (1) activate the PI3K pathway in macrophages, leading to the upregulation of MMPs expression, and (2) promote ECM remodeling and angiogenesis. Together with the enhanced migratory and invasive capacities of LMO1-overexpressing NB cells (as shown previously[14]), these processes collectively drive NB metastasis.

metastasis by regulating the biogenesis of different RNA species, such as rRNA, tiRNA and miRNA,[43] in tumor cells. In addition, the inhibition of Angiopoietin-2 and its commonly known angiogenic partner VEGF can reduce metastasis in patients with breast and lung cancers.[30,44] Other than direct effects on tumor cells, tumor-secreted cytokines also alter the behaviors and functions of immune cells within the TME, such as reducing the amount of functional immune cells and inducing immune exhaustion. TAMs are often one of the most abundant myeloid cells in TMEs and have been extensively studied.[45] The ligand-receptor interactions between HGF and the Met receptor,[31] and between CXCL12 and the CXCR4 receptor,[32] in macrophages have proven roles in facilitating tumor dissemination and aggressiveness by stimulating various oncogenic pathways in tumor cells, including PI3K/Akt, RAS/MAPK, JAK/STAT, SRC, and WNT/β-catenin. Tumor-cell-derived cytokines, such as CCL2, CXCL12, VEGFA, and HGF, are essential for the recruitment of monocytes and macrophages to the tumor site, and CCL2 is important for inducing pro-tumoral activity of recruited macrophages. Elevated levels of CXCL12 are also associated with increased chemorepellent functions of CXCR4-expressing cytotoxic T cells, leading to immune evasion.[46] Hence, the upregulation of these cytokines in LMO1-overexpressing BE2C cells and *MYCN:LMO1* NB tumors could suggest a more immunosuppressive environment stimulated by interactions between tumor and immune cells that favor NB-cell metastasis.

While macrophages play a vital role in tumor metastasis, additional immune cells are involved in TME modification and tumor progression as well. Immune cells apart from macrophages may promote tumorigenesis and metastasis, including neutrophils, NK cells, immature dendritic cells, T cells, invariant NKT cells, and B cells.[47] Although neutrophils have been highly associated with tumor progression and metastasis, elevated levels of NK cells show an anti-tumoral effect and favorable outcomes in certain carcinomas, such as gastric cancer.[48] Additional studies highlight how neutrophils and NK cells can alter the TME to promote or inhibit tumor development, respectively, through immunoediting, which can be used to develop new immunotherapies for highly metastatic cancers.[49] Interestingly, we found in the current study that distinct clusters of neutrophils (8) and NK cells (9) were present in our pooled single-cell transcriptomic analysis of *MYCN* and *MYCN;LMO1* zebrafish tumors (Figures 1A and 1E; Table S7). While cluster 8 contained neutrophils originating from both *MYCN* and *MYCN;LMO1* transgenic zebrafish, the majority of NK cells in cluster 9 originated from *MYCN;LMO1* fish, suggesting that *MYCN;LMO1* NBs may recruit more NK cells for tumor-cell clearance. However, additional studies are needed to clarify the roles and mechanisms of other immune cells, such as

neutrophils and NK cells, during neuroblastomagenesis and metastasis.

Here, we characterized a subset of macrophages present in zebrafish NB with the transgenic overexpression of LMO1 that may enhance metastasis through ECM degradation and PI3K-Akt pathway activation. In patients with NB, LMO1-induced NB may have an elevated level of cytokines that could promote tumor-cell metastasis and alter macrophage functionality. It may therefore be possible to advance cancer therapeutics for patients with NB using macrophages as an alternative immunotherapy. Indeed, recent studies have shown the potential for genetically engineered macrophages (GEMs) in treating cancer. Chimeric antigen receptor macrophages (CAR-M) have been developed and are currently being tested in human clinical trials for the treatment of HER2-overexpressing solid tumors, including lung, breast and gastric cancer (NCT04660929). Unlike CAR T cell therapy, CAR-M therapy is less cytotoxic and has shown more favorable outcomes in patients.[50] These findings underline the promise and potential of macrophage-related immunotherapy. Thus, the design of effective new NB treatments involving the combination of macrophage therapy with LMO1 blockade could improve outcomes for patients with high-risk LMO1-driven NB and possibly prevent the development of metastasis altogether.

Limitations of the study

Although our *in vivo* and *in vitro* data consistently demonstrate that LMO1 overexpression in neuroblastoma cells alters macrophage behavior, several limitations should be acknowledged. First, the mechanistic insights derived from our scRNA-seq analyses are constrained by the limited number of tumor samples and the modest transcriptomic depth of the dataset, which may have prevented the detection of more subtle signaling alterations. Second, incomplete conservation and annotation of zebrafish genes restricted our ability to rigorously define macrophage polarization states, particularly with respect to canonical M1/M2 signatures. Third, although our data supports a role for tumor-secreted cytokines in modulating macrophage activity, we were unable to fully validate these effects within the zebrafish model. Future studies using additional *in vivo* systems with deeper transcriptional profiling and expanded cytokine validation will be essential to further elucidate the tumor-immune interactions mediated by LMO1.

RESOURCE AVAILABILITY

Lead contact

Further information and requests for resources and reagents should be directed to and will be fulfilled by the Lead Contact, Shizhen Zhu (zhu.shizhen@mayo.edu).

Materials availability

This study did not generate new unique reagents.

Data and code availability

The scRNA-seq data are deposited in NCBI with the GEO accession of GSE285755. Further information is available from the corresponding author upon request. This article does not report original code. Any additional information required to reanalyze the data reported in this article is available from the lead contact upon request.

ACKNOWLEDGMENTS

This work was supported by an R01 grant CA240323 (S.Z.) from the National Cancer Institute (NCI) (S.Z.), grants U19AG74879, P50CA136393, OD038392 (H.L.) from the National Institutes of Health (NIH); a United States Department of Defense (DoD) grant W81XWH-17-1-0498 (S.Z.); grants from the Mayo Clinic CBD, Center for Individualized Medicine and the Mayo Clinic Comprehensive Cancer Center (NIH P30CA015083) (H.L.), the Mayo Clinic Center for Cell Signaling in Gastroenterology (NIH P30DK084567) (H.L.); Team Science Awards from the Mayo Clinic Center for Clinical and Translational Science (CCaTS), Center for Biomedical Discovery (CBD) and Mayo Clinic DERIVE Office (S.Z.); supports from Mayo Clinic Comprehensive Cancer Center (S.Z. and H.L.), the Mayo Clinic Center for Individualized Medicine (S.Z. and H.L.), Mayo Clinic Nutrition Obesity Research Program (H.L.), the Glenn Foundation for Medical Research (H.L.), and the Eric & Wendy Schmidt Fund for AI Research & Innovation (H.L.); a V Scholar All-Star award (AST2023-005) from the V Foundation for Cancer Research (S.Z.). We appreciate the comments and edits from Dr. Cicely Jette.

AUTHOR CONTRIBUTIONS

K.T.: investigation, visualization, methodology, and writing – review and editing; Z.P.H.: investigation, visualization, methodology, and writing; C.Z.: investigation and methodology; K.S.Y.: investigation, visualization, methodology, and writing – review and editing; T.W.: investigation and methodology; C.H.: investigation and methodology; S.H.T.: investigation and methodology; K.M.J.: investigation and methodology, G.L.R.: investigation and methodology; R.T.: investigation and methodology; H.L.: investigation and writing – review and editing; S.Z.: conceptualization, data curation, supervision, funding acquisition, project administration, and writing – review and editing.

DECLARATION OF INTERESTS

The authors declare no competing interests.

STAR★METHODS

Detailed methods are provided in the online version of this paper and include the following:

- KEY RESOURCES TABLE
- EXPERIMENTAL MODEL AND STUDY PARTICIPANT DETAILS
  - Zebrafish
  - Cell culture
- METHOD DETAILS
  - Single-cell RNA sequencing (scRNA-seq) and analysis
  - RNA isolation and quantitative RT-PCR
  - Gelatin degradation assay
  - Western blotting analysis
  - Zebrafish xenograft assay
  - Cytokine arrays
- QUANTIFICATION AND STATISTICAL ANALYSIS

SUPPLEMENTAL INFORMATION

Supplemental information can be found online at https://doi.org/10.1016/j.isci.2026.115144.

Received: June 17, 2025
Revised: December 19, 2025
Accepted: February 23, 2026
Published: February 25, 2026

REFERENCES

1. Park, J.R., and Bagatell, R. (2016). Chapter 24 - Neuroblastoma. In Lanzkowsky's Manual of Pediatric Hematology and Oncology, Sixth Edition, P.

Lanzkowsky, J.M. Lipton, and J.D. Fish, eds. (Academic Press), pp. 473–490. https://doi.org/10.1016/B978-0-12-801368-7.00024-7.

2. Maris, J.M., Hogarty, M.D., Bagatell, R., and Cohn, S.L. (2007). Neuroblastoma. Lancet *369*, 2106–2120. https://doi.org/10.1016/S0140-6736(07)60983-0.

3. Morgenstern, D.A., Bagatell, R., Cohn, S.L., Hogarty, M.D., Maris, J.M., Moreno, L., Park, J.R., Pearson, A.D., Schleiermacher, G., Valteau-Couanet, D., et al. (2019). The challenge of defining ''ultra-high-risk'' neuroblastoma. Pediatr. Blood Cancer *66*, e27556. https://doi.org/10.1002/pbc.27556.

4. He, S., Mansour, M.R., Zimmerman, M.W., Ki, D.H., Layden, H.M., Akahane, K., Gjini, E., de Groh, E.D., Perez-Atayde, A.R., Zhu, S., et al. (2016). Synergy between loss of NF1 and overexpression of MYCN in neuroblastoma is mediated by the GAP-related domain. eLife *5*, e14713. https://doi.org/10.7554/eLife.14713.

5. Matthay, K.K., Maris, J.M., Schleiermacher, G., Nakagawara, A., Mackall, C.L., Diller, L., and Weiss, W.A. (2016). Neuroblastoma. Nat. Rev. Dis. Primers *2*, 16078. https://doi.org/10.1038/nrdp.2016.78.

6. Li, S., Yeo, K.S., Levee, T.M., Howe, C.J., Her, Z.P., and Zhu, S. (2021). Zebrafish as a Neuroblastoma Model: Progress Made, Promise for the Future. Cells *10*, 580.

7. Bhavsar, S.P. (2023). Metastasis in neuroblastoma: the MYCN question. Front. Oncol. *13*, 1196861. https://doi.org/10.3389/fonc.2023.1196861.

8. Wang, K., Diskin, S.J., Zhang, H., Attiyeh, E.F., Winter, C., Hou, C., Schnepp, R.W., Diamond, M., Bosse, K., Mayes, P.A., et al. (2011). Integrative genomics identifies LMO1 as a neuroblastoma oncogene. Nature *469*, 216–220. https://doi.org/10.1038/nature09609.

9. Oldridge, D.A., Wood, A.C., Weichert-Leahey, N., Crimmins, I., Sussman, R., Winter, C., McDaniel, L.D., Diamond, M., Hart, L.S., Zhu, S., et al. (2015). Genetic predisposition to neuroblastoma mediated by a LMO1 super-enhancer polymorphism. Nature *528*, 418–421. https://doi.org/10.1038/nature15540.

10. Gerby, B., Tremblay, C.S., Tremblay, M., Rojas-Sutterlin, S., Herblot, S., Hébert, J., Sauvageau, G., Lemieux, S., Lécuyer, E., Veiga, D.F.T., and Hoang, T. (2014). SCL, LMO1 and Notch1 reprogram thymocytes into self-renewing cells. PLoS Genet. *10*, e1004768. https://doi.org/10.1371/journal.pgen.1004768.

11. Tan, S.H., Bertulfo, F.C., and Sanda, T. (2017). Leukemia-Initiating Cells in T-Cell Acute Lymphoblastic Leukemia. Front. Oncol. *7*, 218. https://doi.org/10.3389/fonc.2017.00218.

12. Zhao, G.F., Du, L.Q., Zhang, L., and Jia, Y.C. (2021). LIM domain only 1: an oncogenic transcription cofactor contributing to the tumorigenesis of multiple cancer types. Chin. Med. J. *134*, 1017–1030. https://doi.org/10.1097/cm9.0000000000001487.

13. Xie, Y., Wang, A., Lin, J., Wu, L., Zhang, H., Yang, X., Wan, X., Miao, R., Sang, X., and Zhao, H. (2017). Mps1/TTK: a novel target and biomarker for cancer. J. Drug Target. *25*, 112–118. https://doi.org/10.1080/1061186x.2016.1258568.

14. Zhu, S., Zhang, X., Weichert-Leahey, N., Dong, Z., Zhang, C., Lopez, G., Tao, T., He, S., Wood, A.C., Oldridge, D., et al. (2017). LMO1 Synergizes with MYCN to Promote Neuroblastoma Initiation and Metastasis. Cancer Cell *32*, 310–323.e5. https://doi.org/10.1016/j.ccell.2017.08.002.

15. Ponzoni, M., Bachetti, T., Corrias, M.V., Brignole, C., Pastorino, F., Calarco, E., Bensa, V., Giusto, E., Ceccherini, I., and Perri, P. (2022). Recent advances in the developmental origin of neuroblastoma: an overview. J. Exp. Clin. Cancer Res. *41*, 92. https://doi.org/10.1186/s13046-022-02281-w.

16. Hald, Ø.H., Olsen, L., Gallo-Oller, G., Elfman, L.H.M., Løkke, C., Kogner, P., Sveinbjörnsson, B., Flægstad, T., Johnsen, J.I., and Einvik, C. (2019). Inhibitors of ribosome biogenesis repress the growth of MYCN-amplified neuroblastoma. Oncogene *38*, 2800–2813. https://doi.org/10.1038/s41388-018-0611-7.

17. Matthews, J.M., Lester, K., Joseph, S., and Curtis, D.J. (2013). LIM-domain-only proteins in cancer. Nat. Rev. Cancer *13*, 111–122. https://doi.org/10.1038/nrc3418.

18. Jouines, C., Lo Monaco, P., Gaucherot, A., Monet, M.A., Iacono Di Cacito, I., Simioni, V., Monchiet, D., Diaz, J.J., Combaret, V., Marcel, V., and Catez, F. (2025). Ribosome biogenesis is a therapeutic vulnerability in pediatric neuroblastoma. Biochimie *238*, 73–83. https://doi.org/10.1016/j.biochi.2025.07.018.

19. Jahangiri, L. (2024). Metabolic targeting of neuroblastoma, an update. Cancer Lett. *611*, 217393. https://doi.org/10.1016/j.canlet.2024.217393.

20. van Riggelen, J., Yetil, A., and Felsher, D.W. (2010). MYC as a regulator of ribosome biogenesis and protein synthesis. Nat. Rev. Cancer *10*, 301–309. https://doi.org/10.1038/nrc2819.

21. Wolf, A., Leardini, D., Li, L., Masetti, R., Lyssiotis, C.A., and Barbieri, E. (2026). Deciphering the MYCN-driven metabolic microenvironment of neuroblastoma. Trends Mol. Med. *32*, 166–180. https://doi.org/10.1016/j.molmed.2025.08.005.

22. Farnsworth, D.R., Saunders, L.M., and Miller, A.C. (2020). A single-cell transcriptome atlas for zebrafish development. Dev. Biol. *459*, 100–108. https://doi.org/10.1016/j.ydbio.2019.11.008.

23. Wang, S., Wang, J., Chen, Z., Luo, J., Guo, W., Sun, L., and Lin, L. (2024). Targeting M2-like tumor-associated macrophages is a potential therapeutic approach to overcome antitumor drug resistance. npj Precis. Oncol. *8*, 31. https://doi.org/10.1038/s41698-024-00522-z.

24. Aizaz, M., Khan, A., Khan, F., Khan, M., Musad Saleh, E.A., Nisar, M., and Baran, N. (2023). The cross-talk between macrophages and tumor cells as a target for cancer treatment. Front. Oncol. *13*, 1259034. https://doi.org/10.3389/fonc.2023.1259034.

25. Bied, M., Ho, W.W., Ginhoux, F., and Blériot, C. (2023). Roles of macrophages in tumor development: a spatiotemporal perspective. Cell. Mol. Immunol. *20*, 983–992. https://doi.org/10.1038/s41423-023-01061-6.

26. Luyendyk, J.P., Schabbauer, G.A., Tencati, M., Holscher, T., Pawlinski, R., and Mackman, N. (2008). Genetic analysis of the role of the PI3K-Akt pathway in lipopolysaccharide-induced cytokine and tissue factor gene expression in monocytes/macrophages. J. Immunol. *180*, 4218–4226. https://doi.org/10.4049/jimmunol.180.6.4218.

27. Lu, Y., and Wahl, L.M. (2005). Production of matrix metalloproteinase-9 by activated human monocytes involves a phosphatidylinositol-3 kinase/Akt/IKKalpha/NF-kappaB pathway. J. Leukoc. Biol. *78*, 259–265. https://doi.org/10.1189/jlb.0904498.

28. Yu, Y., Savage, R.E., Eathiraj, S., Meade, J., Wick, M.J., Hall, T., Abbadessa, G., and Schwartz, B. (2015). Targeting AKT1-E17K and the PI3K/AKT Pathway with an Allosteric AKT Inhibitor, ARQ 092. PLoS One *10*, e0140479. https://doi.org/10.1371/journal.pone.0140479.

29. Morris, R.M., Mortimer, T.O., and O'Neill, K.L. (2022). Cytokines: Can Cancer Get the Message? Cancers (Basel) *14*. https://doi.org/10.3390/cancers14092178.

30. Bohn, K.A., Adkins, C.E., Nounou, M.I., and Lockman, P.R. (2017). Inhibition of VEGF and Angiopoietin-2 to Reduce Brain Metastases of Breast Cancer Burden. Front. Pharmacol. *8*, 193. https://doi.org/10.3389/fphar.2017.00193.

31. Nishikoba, N., Kumagai, K., Kanmura, S., Nakamura, Y., Ono, M., Eguchi, H., Kamibayashiyama, T., Oda, K., Mawatari, S., Tanoue, S., et al. (2020). HGF-MET Signaling Shifts M1 Macrophages Toward an M2-Like Phenotype Through PI3K-Mediated Induction of Arginase-1 Expression. Front. Immunol. *11*, 2135. https://doi.org/10.3389/fimmu.2020.02135.

32. Raschioni, C., Bottai, G., Sagona, A., Errico, V., Testori, A., Gatzemeier, W., Corsi, F., Tinterri, C., Roncalli, M., Santarpia, L., and Di Tommaso, L. (2018). CXCR4/CXCL12 Signaling and Protumor Macrophages in Primary Tumors and Sentinel Lymph Nodes Are Involved in Luminal B Breast Cancer Progression. Dis. Markers *2018*, 5018671. https://doi.org/10.1155/2018/5018671.

33. Otte, J., Dyberg, C., Pepich, A., and Johnsen, J.I. (2020). MYCN Function in Neuroblastoma Development. Front. Oncol. *10*, 624079. https://doi.org/10.3389/fonc.2020.624079.

34. Liu, Z., and Thiele, C.J. (2017). When LMO1 Meets MYCN, Neuroblastoma Is Metastatic. Cancer Cell *32*, 273–275. https://doi.org/10.1016/j.ccell.2017.08.014.

35. Morgia, G., Falsaperla, M., Malaponte, G., Madonia, M., Indelicato, M., Travali, S., and Mazzarino, M.C. (2005). Matrix metalloproteinases as diagnostic (MMP-13) and prognostic (MMP-2, MMP-9) markers of prostate cancer. Urol. Res. *33*, 44–50. https://doi.org/10.1007/s00240-004-0440-8.

36. Lin, Y., Xu, J., and Lan, H. (2019). Tumor-associated macrophages in tumor metastasis: biological roles and clinical therapeutic applications. J. Hematol. Oncol. *12*, 76. https://doi.org/10.1186/s13045-019-0760-3.

37. Yang, D., Yang, L., Cai, J., Li, H., Xing, Z., and Hou, Y. (2022). Phosphoinositide 3-kinase/Akt and its related signaling pathways in the regulation of tumor-associated macrophages polarization. Mol. Cell. Biochem. *477*, 2469–2480. https://doi.org/10.1007/s11010-022-04461-w.

38. Lai, Y.S., Wahyuningtyas, R., Aui, S.P., and Chang, K.T. (2019). Autocrine VEGF signalling on M2 macrophages regulates PD-L1 expression for immunomodulation of T cells. J. Cell Mol. Med. *23*, 1257–1267. https://doi.org/10.1111/jcmm.14027.

39. Yang, C.C., Lin, C.C., Hsiao, L.D., Kuo, J.M., Tseng, H.C., and Yang, C.M. (2019). Lipopolysaccharide-Induced Matrix Metalloproteinase-9 Expression Associated with Cell Migration in Rat Brain Astrocytes. Int. J. Mol. Sci. *21*, 259. https://doi.org/10.3390/ijms21010259.

40. Zhao, H.-Y., Zhang, Y.-Y., Xing, T., Tang, S.-Q., Wen, Q., Lyu, Z.-S., Lv, M., Wang, Y., Xu, L.-P., Zhang, X.-H., et al. (2021). M2 macrophages, but not M1 macrophages, support megakaryopoiesis by upregulating PI3K-AKT pathway activity. Signal Transduct. Targeted Ther. *6*, 234. https://doi.org/10.1038/s41392-021-00627-y.

41. Linton, M.F., Moslehi, J.J., and Babaev, V.R. (2019). Akt Signaling in Macrophage Polarization, Survival, and Atherosclerosis. Int. J. Mol. Sci. *20*, 2703. https://doi.org/10.3390/ijms20112703.

42. Yang, Y., Jia, X., Qu, M., Yang, X., Fang, Y., Ying, X., Zhang, M., Wei, J., and Pan, Y. (2023). Exploring the potential of treating chronic liver disease targeting the PI3K/Akt pathway and polarization mechanism of macrophages. Heliyon *9*, e17116. https://doi.org/10.1016/j.heliyon.2023.e17116.

43. Annese, T., Tamma, R., De Giorgis, M., and Ribatti, D. (2020). microRNAs Biogenesis, Functions and Role in Tumor Angiogenesis. Front. Oncol. *10*, 581007. https://doi.org/10.3389/fonc.2020.581007.

44. Minami, T., Jiang, S., Schadler, K., Suehiro, J.I., Osawa, T., Oike, Y., Miura, M., Naito, M., Kodama, T., and Ryeom, S. (2013). The calcineurin-NFAT-angiopoietin-2 signaling axis in lung endothelium is critical for the establishment of lung metastases. Cell Rep. *4*, 709–723. https://doi.org/10.1016/j.celrep.2013.07.021.

45. de Visser, K.E., and Joyce, J.A. (2023). The evolving tumor microenvironment: From cancer initiation to metastatic outgrowth. Cancer Cell *41*, 374–403. https://doi.org/10.1016/j.ccell.2023.02.016.

46. Kohli, K., Pillarisetty, V.G., and Kim, T.S. (2022). Key chemokines direct migration of immune cells in solid tumors. Cancer Gene Ther. *29*, 10–21. https://doi.org/10.1038/s41417-021-00303-x.

47. Gonzalez, H., Hagerling, C., and Werb, Z. (2018). Roles of the immune system in cancer: from tumor initiation to metastatic progression. Genes Dev. *32*, 1267–1284. https://doi.org/10.1101/gad.314617.118.

48. Iannello, A., Thompson, T.W., Ardolino, M., Marcus, A., and Raulet, D.H. (2016). Immunosurveillance and immunotherapy of tumors by innate immune cells. Curr. Opin. Immunol. *38*, 52–58. https://doi.org/10.1016/j.coi.2015.11.001.

49. Póvoa, V., Rebelo de Almeida, C., Maia-Gil, M., Sobral, D., Domingues, M., Martinez-Lopez, M., de Almeida Fuzeta, M., Silva, C., Grosso, A.R., and Fior, R. (2021). Innate immune evasion revealed in a colorectal zebrafish xenograft model. Nat. Commun. *12*, 1156. https://doi.org/10.1038/s41467-021-21421-y.

50. Chen, Y., Yu, Z., Tan, X., Jiang, H., Xu, Z., Fang, Y., Han, D., Hong, W., Wei, W., and Tu, J. (2021). CAR-macrophage: A new immunotherapy candidate against solid tumors. Biomed. Pharmacother. *139*, 111605. https://doi.org/10.1016/j.biopha.2021.111605.

51. Kimmel, C.B., Ballard, W.W., Kimmel, S.R., Ullmann, B., and Schilling, T.F. (1995). Stages of embryonic development of the zebrafish. Dev. Dyn. *203*, 253–310. https://doi.org/10.1002/aja.1002030302.

52. Zhu, S., Lee, J.S., Guo, F., Shin, J., Perez-Atayde, A.R., Kutok, J.L., Rodig, S.J., Neuberg, D.S., Helman, D., Feng, H., et al. (2012). Activated ALK collaborates with MYCN in neuroblastoma pathogenesis. Cancer Cell *21*, 362–373. https://doi.org/10.1016/j.ccr.2012.02.010.

53. Nirmal, A.J., Regan, T., Shih, B.B., Hume, D.A., Sims, A.H., and Freeman, T.C. (2018). Immune Cell Gene Signatures for Profiling the Microenvironment of Solid Tumors. Cancer Immunol. Res. *6*, 1388–1400. https://doi.org/10.1158/2326-6066.Cir-18-0342.

54. Rougeot, J., Torraca, V., Zakrzewska, A., Kanwal, Z., Jansen, H.J., Sommer, F., Spaink, H.P., and Meijer, A.H. (2019). RNAseq Profiling of Leukocyte Populations in Zebrafish Larvae Reveals a cxcl11 Chemokine Gene as a Marker of Macrophage Polarization During Mycobacterial Infection. Front. Immunol. *10*, 832. https://doi.org/10.3389/fimmu.2019.00832.

55. Mi, H., Muruganujan, A., Huang, X., Ebert, D., Mills, C., Guo, X., and Thomas, P.D. (2019). Protocol Update for large-scale genome and gene function analysis with the PANTHER classification system (v.14.0). Nat. Protoc. *14*, 703–721. https://doi.org/10.1038/s41596-019-0128-8.

56. Love, M.I., Huber, W., and Anders, S. (2014). Moderated estimation of fold change and dispersion for RNA-seq data with DESeq2. Genome Biol. *15*, 550. https://doi.org/10.1186/s13059-014-0550-8.

57. Hänzelmann, S., Castelo, R., and Guinney, J. (2013). GSVA: gene set variation analysis for microarray and RNA-seq data. BMC Bioinf. *14*. https://doi.org/10.1186/1471-2105-14-7.

STAR★METHODS

KEY RESOURCES TABLE

REAGENT or RESOURCE	SOURCE	IDENTIFIER
Antibodies		
MMP9	Cell Signaling Technology	Cat#3852S, RRID:AB_2144868
MMP14	Abcam	ab51074, RRID:AB_881234
MMP13	Santa Cruz	H-230, RRID:AB_2145167
Phospho-Akt (Ser-473)	Cell Signaling Technology	Cat# 4058S, RRID:AB_331168
Pan Akt Antibody (C67E7)	Cell Signaling Technology	Cat# 4691L, RRID:AB_915783
GAPDH	GeneTex	GTX100118, RRID:AB_1080976
Goat anti-Rabbit IgG (H + L) Secondary Antibody, HRP	Thermo Fisher Scientific	Cat#31460, RRID:AB_228341
Goat anti-Mouse IgG (H + L) Secondary Antibody	Thermo Fisher Scientific	Cat#31160, RRID:AB_228297
Chemicals, peptides, and recombinant proteins		
Oregon Green-488 Gelatin	Invitrogen	Cat#G13186
Miransertib	Selleckchem	Cat#S8339
Critical commercial assays		
NucleoSpin RNA plus kit	Macherey-Nagel	Cat# 740984.250
Moloney Murine Leukemia Virus (M-MuLV, MMLV) Reverse Transcriptase	New England Biolabs	Cat# M0253L
Proteome Profiler Human XL Cytokine Array Kit	R&D Systems	Cat#ARY022B
Deposited Data		
scRNA-seq data	This paper	NCBI: GSE285755
Experimental models: Cell lines		
BE2C	ATCC	Cat# CRL-2268, RRID: CVCL_0529
U937	ATCC	Cat# CRL-1593.2, RRID:CVCL_0007
Experimental models: Organisms/strains		
Zebrafish AB	ZIRC	Cat# ZL1, RRID: ZIRC_ZL1
Zebrafish:Tg(*dbh:EGFP-Hsa.MYCN*): zdf16Tg	(48)	ZFIN: ZDB-ALT-120409-3
Zebrafish:Tg(*dbh:LMO1;dbh:mCherry*): zdf33Tg	(15)	ZFIN: ZDB-ALT-171212-6
Oligonucleotides		
Primers for qPCR, see Table S8	This paper	N/A
Software and algorithms		
GraphPad Prism10	GraphPad software	www.graphpad.com
ImageJ	NIH	http://rsbweb.nih.gov/ij/
AdobePhotoshop CS	Adobe software	http://www.adobe.com/products/photoshop.html
Excel	Microsoft	https://www.microsoft.com/
ImageQuant™ TL	Cytiva	https://www.cytivalifesciences.com

EXPERIMENTAL MODEL AND STUDY PARTICIPANT DETAILS

Zebrafish

The zebrafish studies were conducted in accordance with Mayo Clinic Institutional Animal Care and Use Committee (IACUC)-approved protocol #A00004637-19-R22 and the *Guide for the Care and Use of Laboratory Animals*. Fish were maintained in a

centralized aquatic facility under standard conditions (28.5°C; 14-hour light/10-hour dark cycle) in a recirculating water system and were fed a standard laboratory diet appropriate for developmental stage. All zebrafish used in this study were derived from the AB background strain, and embryos/juvenile fish were staged according to Kimmel et al.[51] Transgenic zebrafish lines *MYCN* and *MYCN;LMO1* were generated and validated by fluorescence-based sorting and genotyping zebrafish as described in our previous publications.[14,52] For experimental analyses, 6∼8-month-old adult heterozygous male and female fish from both transgenic lines were randomly selected for single-cell RNA sequencing. Sex was included as a biological variable in the analysis; however, no significant sex-specific differences were observed in the measured outcomes. Notably, metastasis of NB cells was detected by microscopy in *MYCN;LMO1* tumor fish, whereas metastasis was not observed in *MYCN*-only fish.

Cell culture

The human neuroblastoma cell line BE2C (ATCC Cat# CRL-2268, RRID: CVCL_0529) and the U937 (ATCC Cat# CRL-1593.2, RRID:CVCL_0007) human monocytes were obtained from the American Type Culture Collection (ATCC). All cell lines were authenticated using short tandem repeat (STR) profiling within the last three years and all experiments were performed with mycoplasma-free cells. These cells were cultured in RPMI 1640 media (Gibco, #61870-036) supplemented with 10% heat-inactivated FBS (Gibco, #A5256801) and 1× Antibiotic-Antimycotic (Gibco, #10131027). All cells were cultured at 37°C in a 5% CO_2 incubator. Approximately 8×10^5 Ctl BE2C and LMO1-overexpressing BE2C cells were seeded in 6-well plates and incubated for 48 h prior to conditioned media (CM) collection. Upon collection, CM was centrifuged at 500 × g and either used immediately or stored at -80°C until use. Before CM treatment, approximately 1×10^6 U937 cells were seeded in 6-well plates and differentiated to macrophages with 20 ng/mL phorbol 12-myristate 13-acetate (PMA) (Sigma-Aldrich, #P1585) for 24 h. Differentiated U937 cells were rinsed with 1× PBS prior to treatment with collected CM for 48 h.

METHOD DETAILS

Single-cell RNA sequencing (scRNA-seq) and analysis

A Fluidigm C1 system was used to capture single cells dissociated from zebrafish tumors. cDNA libraries from single cells were prepared using the SMART-seq strategy and subjected to Illumina Hi-Seq sequencing at the Harvard Medical School Biopolymers Facility. A total of 16,630 cells were sequenced, and 9,082 high-quality transcriptomes were obtained after quality control and filtering from the 5 tumor samples. The sequencing coverage and quality statistics for each sample are summarized in Table S1.

Fastq files were output in the inDrops v3 format and aligned as described by the inDrops pipeline [https://github.com/indrops/indrops]. A customized reference genome was created by integrating the zebrafish reference genome GRCz11 plus the transgenic sequences of *MYCN* and *LMO1* transgenes. The output gene-barcode matrices from the inDrops pipeline were used as input for the R package Seurat version 3.2.3. To remove low-quality cells, bar codes (cells) were filtered to have > 500 unique genes mapped with total UMI counts > 1000, and mitochondrial RNA content < 10%. Genes that were only expressed in 3 or fewer cells were discarded. Raw counts were log-transformed and multiplied by a factor of 1000. Variable features were identified as top 2000 genes with high variance across all the cells, and principal component analysis (PCA) was performed on these variable features after being centered, scaled and the number of UMI of each cell regressed out. An elbow plot showing number of principal components (PCs) vs. cumulative total variance explained was produced and top 10 PCs were considered optimal for downstream analysis. Cells were grouped into clusters using the Louvain algorithm with a resolution of 0.6.

Cell types were determined by using respective marker gene sets and the SciBet algorithm.[53,54] Cluster and genotype (*MYCN* versus *MYCN:LMO1*) marker genes were determined by 1) using function ''FindAllMarkers'' for each group, 2) filtering genes by Bonferroni-corrected p-value < 0.05 and $\log_2$ fold-change > 0.25, and 3) gene expression in at least 25% of cells in the cluster.

To assess difference in functional enrichment of different genotypes, differentially expressed genes with FDR < 0.05 were extracted from each comparison, split into gene lists with positive and negative $\log_2$ fold-changes and then uploaded for over-representation tests against gene ontology gene sets.[55] Significantly enriched pathways with similar GO term were aggregated into broader functional groups, and the $-\log_{10}$ FDR values for each pathway within each group were plotted in violin plot with the cutoff of $-\log_{10}$ FDR > 2.

Pseudobulk gene expression profiles were created by aggregating raw counts of each cell from the same library. These pseudobulk profiles were analyzed using the DESeq2 package with default parameters.[56] Gene set variation analysis (GSVA) was performed according to.[57]

RNA isolation and quantitative RT-PCR

Total RNA was isolated with a Macherey Nagel NucleoSpin® RNA kit, and random hexamer-converted cDNA was synthesized using M-MuLV reverse transcriptase (NEB, #M0253L) according to the manufacturer's protocol. Quantitative reverse-transcription polymerase chain reaction (RT-qPCR) was performed using 2 × PerfeCTa® SYBR® Green SuperMix (Quantabio, Cat# 95054-02K) according to the manufacturer's protocol and run on a Bio-Rad Duet Real-Time PCR System. Expression fold-change was normalized using *SDHA* as a housekeeping gene and calculated using the comparative Ct method ($2^{-\Delta\Delta Ct}$). The list of primers used for RT-qPCR is included in Table S8.

Gelatin degradation assay

Differentiated and CM-treated U937 macrophages were labeled with ViaFluor 405 and seeded at a density of 5×10^4 cells per well in a 12-well plate with a coverslip (Fisher Scientific, Cat# 12541A) coated with Oregon Green-488 Gelatin (Invitrogen, #G13186). Cells were incubated in 5% CO_2 at 37°C for 4-6 h and fixed with 4% paraformaldehyde. Nuclei were stained with DAPI (Biolegend, #422801). Coverslips were imaged with Nikon Ti2-E widefield fluorescent microscope. Areas of gelatin degradation by the macrophages appeared as non-fluorescent dark spots under a fluorescent microscope, indicating regions where the gelatin matrix had been degraded. At least five random fields per sample were captured for analysis using fluorescence microscopy. ImageJ software was then used to differentiate degraded (black) regions from intact (green) gelatin areas. The percentage of gelatin degradation was calculated by determining the ratio of degraded areas to the number of U937 macrophages present in each field.

Western blotting analysis

Harvested cells were lysed with IPKA lysis buffer (20 mM Tris pH 7.5, 150 mM NaCl, 10% glycerol, 1% Triton-X) supplemented with 1× protease-inhibitor cocktail, 1× phosphatase-inhibitor cocktail, 1 mM sodium orthovanadate, 1 mM phenylmethylsulphonyl fluoride (PMSF), 1 mM dichloro-diphenyl-trichloroethane (DDT) and 25 mM β-glycerol-phosphate. Cell lysate was then incubated on ice for 30 min with occasional disturbance at 5-min intervals. Total cell lysate was collected by centrifugation at max speed for 15 min at 4°C. Primary antibodies against MMP9 (3852S, RRID:AB_2144868), pAkt (4058S, RRID:AB_331168) and total Akt (4691L, RRID:AB_915783), MMP14 (ab51074, RRID:AB_881234), MMP13 (H-230, RRID:AB_2145167), and GAPDH (GTX100118, RRID:AB_1080976) were acquired from Cell Signaling Technology, Abcam, Santa Cruz and GeneTex respectively. Rabbit IgG (H+L) secondary antibody (31460, RRID:AB_228341) and goat anti-mouse IgG (H+L) secondary antibody (31160, RRID:AB_228297) were purchased from Thermo Fisher Scientific. Immunoblotting images were captured using ImageQuant 800 systems (Amersham). Protein band intensities were quantified using ImageJ. Expression levels were first normalized to the corresponding housekeeping control and then expressed relative to the control-treated groups.

Zebrafish xenograft assay

mCherry-labeled human NB BE2C cells were co-injected with ViaFlour-405-fluorescent-dye-labeled, differentiated, and CM-treated human U937 macrophages into the perivitelline space (PVS) of 2-day-old AB wildtype zebrafish embryos that were being treated continuously with 0.003% 1-phenyl 2-thiourea (PTU) starting at 24 h post-fertilization. At 1 day post injection (dpi), zebrafish embryos were screened randomly and imaged with an upright fluorescent microscope. To minimize handling and reduce larval mortality, we chose to acquire one lateral and one dorsal image per fish at 10× magnification, focusing on the injection site and head region where early migration events are most consistently observed. At 3-4 dpi, zebrafish xenografts were imaged again to analyze migration of the mCherry-labeled BE2C cells. Migration of BE2C cells in co-transplanted xenografts was defined at 3 dpi as at least one or more mCherry-positive cells located distant from the original site of injection.

Cytokine arrays

Cytokines were detected and measured in the CM from Ctl BE2C and LMO1-overexpressing BE2C cells using the Proteome Profiler Human XL Cytokine Array Kit (R&D Systems, #ARY022B) according to the manufacturer's instructions. Signal intensities for the cytokine array blots were calculated by Cytiva ImageQuant™ TL 10.2 analysis software.

QUANTIFICATION AND STATISTICAL ANALYSIS

Data was analyzed using GraphPad Prism 10.1.2 and presented as mean ± SD. Data are representative of at least two independent experiments. Statistically significant p values [≤ 0.05 (*), ≤ 0.01 (**), ≤ 0.001 (***) and ≤ 0.0001 (****)] were determined by student's t-test.